Title

Rapid, concurrent formation of organic sulfur and iron sulfides during experimental sulfurization of sinking marine particles

Authors

Raven, Morgan
Keil, Richard G
Webb, Samuel M

Publication Date

2021-05-10

DOI

10.1002/essoar.10506986.1

Rapid, concurrent formation of organic sulfur and iron sulfides during experimental sulfurization of sinking marine particles

M. R. Raven[1*], R. G. Keil[2], S. M. Webb[3]

[1] Department of Earth Science, University of California, Santa Barbara, Santa Barbara CA 93117, USA

[2] School of Oceanography, University of Washington, Seattle WA 98195, USA

[3] Stanford Synchrotron Radiation Lightsource, Stanford University, Menlo Park CA 94025, USA

Corresponding Author: Morgan Reed Raven (raven@ucsb.edu)

Key Points:

1. Organic matter in sinking marine particles sulfurizes rapidly in the presence of polysulfides, tripling its S:C ratio in 48 hours.

2. Iron monosulfides form from iron oxyhydroxide particles on the same timescale as organic sulfur.

3. Organic matter sulfurization in sinking particles may increase carbon burial in sediments, impacting sedimentary records and climate.

Abstract

Organic matter (OM) sulfurization can enhance the preservation and sequestration of carbon in anoxic sediments, and it has been observed in sinking marine particles from marine O_2-deficient zones. The magnitude of this effect on carbon burial remains unclear, however, because the transformations that occur when sinking particles encounter sulfidic conditions remain undescribed. Here, we briefly expose sinking marine particles from the eastern tropical North Pacific O_2-deficient zone to environmentally relevant sulfidic conditions (20°C, 0.5 mM [poly]sulfide, two days) and then characterize the resulting solid-phase organic and inorganic products in detail. During these experiments, the abundance of organic sulfur in both hydrolyzable and hydrolysis-resistant solids roughly triples, indicating extensive OM sulfurization. Lipids also sulfurize on this timescale, albeit less extensively. In all three pools, OM sulfurization produces organic monosulfides, thiols, and disulfides. Hydrolyzable sulfurization products appear within ≤ 200-μm regions of relatively homogenous composition that are suggestive of sulfurized extracellular polymeric substances (EPS). Concurrently, reactions with particulate iron oxyhydroxides generate low and fairly uniform concentrations of iron sulfide (FeS) within these same EPS-like materials. Iron oxyhydroxides were not fully consumed during the experiment, which demonstrates that organic materials can be competitive with reactive iron for sulfide. These experiments support the hypothesis that sinking, OM- and EPS-rich particles in a sulfidic water mass can sulfurize within days, potentially contributing to enhanced sedimentary carbon sequestration. Additionally, sulfur-isotope and chemical records of organic S and iron sulfides in sediments have the potential to incorporate signals from water column processes.

Plain Language Summary

Vast amounts of organic carbon are stored in sediments on the ocean floor. This organic carbon is potentially food for macro- and microorganisms, and yet, under specific environmental conditions, it can escape being eaten and instead persist in sediments and rocks for millions of years. Here, we conduct experiments that test how the organic and inorganic materials in sinking marine particles can be

41 transformed by two days of exposure to sulfidic environmental conditions, which are often associated
42 with high rates of organic carbon burial in sediments. We find that these sulfidic conditions substantially
43 alter the chemistry of ("pickle") particle organic materials, yielding products that resemble preserved
44 organic materials in ancient deposits. Marine particles that encounter sulfidic conditions in the
45 environment are therefore more likely to be preserved and buried in sediments, sequestering carbon out of
46 the ocean and atmosphere. This process, called 'sulfurization,' may act as a stabilizing feedback in the
47 carbon cycle as ocean anoxic zones expand in response to ongoing climate change.
48
49
50 **1. Introduction**

51 In most of the surface ocean today, photosynthetic algae and bacteria produce organic matter (OM)
52 that is cycled efficiently and locally through metabolic networks linking bacteria, viruses, zooplankton, and
53 their exudates. OM may also become incorporated into aggregates with sufficient density to sink, or it can
54 be transported out of the mixed layer by other particle "pumps" (Boyd et al., 2019). Large (≥ ~1 mm),
55 sinking particles may travel thousands of meters to the seafloor in a few days (La Rocha and Passow, 2007).
56 As particles sink, they are continually used as a food source, so the downward flux of sinking particulate
57 OM is strongly attenuated with depth due to oxic respiration. As a result, only a tiny fraction (~1.5%) of
58 global marine primary production is buried in sediments. In contrast, the efficiency of OM burial can be
59 much higher in certain types of near-shore (coastal, shelf, or borderland basin) environments (Dunne et al.,
60 2007; Bianchi et al., 2018), especially those with low dissolved O_2 concentrations like the O_2-deficient
61 zones (ODZs) of the Eastern Tropical Pacific and Arabian Sea (Martin et al., 1987; Devol and Hartnett,
62 2001; B. Van Mooy et al., 2002; Hartnett and Devol, 2003; Keil et al., 2016). Under the more strongly
63 reducing, frequently sulfidic conditions found in the southern North Atlantic during the Cretaceous ocean
64 anoxic events, OM burial in sediments served as a major sink for CO_2 and likely mitigated a hothouse
65 climate (Arthur et al., 1988; Sinninghe Damsté and Köster, 1998; Hülse et al., 2019). Nonetheless, without

66 a more mechanistic understanding of the underlying causes of enhanced sinking particle fluxes in anoxic
67 environments, we are unable to quantitatively predict how ongoing ODZ expansion and other changes in
68 marine O_2 availability (Deutsch et al., 2011; Stramma et al., 2011; Schmidtko et al., 2017; Breitburg et al.,
69 2018; Takano et al., 2018) will impact carbon fluxes to the sediments.

70 Multiple physical, chemical, and biological mechanisms contribute to the enhanced sinking organic
71 particle flux through anoxic water columns (Keil et al., 2016). Especially in anoxic environments, clays and
72 other minerals physically protect sedimentary OM by occlusion or sorption onto surfaces (Salmon et al.,
73 2000; Arnarson and Keil, 2007). Anaerobic microorganisms also gain less energy from the oxidation of
74 organic matter than aerobic organisms (Froelich et al., 1979), and some individual organic molecules may
75 become energetically inaccessible at certain redox potentials (Boye et al., 2017). However, anoxic
76 sedimentary systems often preserve greater quantities of OM than can be explained by surface protection,
77 microbial energetics, or the availability of alternative electron acceptors like sulfate (Arndt et al., 2013),
78 indicating that there is a role for condensation and kerogenization reactions that render OM inaccessible to
79 microbes and their exoenzymes. A special category of kerogenization reactions that is specific to anoxic
80 environments, OM sulfurization, was observed in sinking ODZ particles under *in-situ* conditions and could
81 be a significant contributor to OM burial (Raven et al., 2021).

82 OM sulfurization reduces the effective lability of OM by replacing certain functional groups (e.g.,
83 aldehydes, conjugated double bonds) with organic S functionalities and by bridging molecules together,
84 increasing their molecular weight (Sinninghe Damsté et al., 1988; Kohnen et al., 1989; Kutuzov et al.,
85 2020). Sulfurized OM is thus less susceptible to breakdown by microbial exoenzymes than fresh or
86 degraded algal biomass (Boussafir and Lallier-Verges, 1997; Sinninghe Damsté and Köster, 1998). The
87 reactants for sulfurization on timescales of days or less appear to be polysulfides (S_x^{2-}, $2 \leq x \leq 8$), which
88 form spontaneously in the presence of dissolved sulfide (HS^-) and elemental S (S^0) or other oxidants
89 (Kamyshny et al., 2004; Rickard and Luther, 2007). In experiments, algal biomass has been shown to
90 sulfurize rapidly in the presence of dissolved polysulfides, producing pyrolysates interpreted as deriving

from carbohydrates cross-linked with organic sulfides and polysulfides (Gelin et al., 1998; Kok, Schouten, et al., 2000; Pohlabeln et al., 2017). Experiments with model compounds have shown similar cross-linking following polysulfide exposure (van Dongen et al., 2003; Amrani and Aizenshtat, 2004a). Over the past few years, OM sulfurization has been reported across a growing diversity of environments, including coastal mangrove forests, hydrothermal systems, marine surface sediments exposed to variable redox conditions (Gomez-Saez et al., 2016; Jessen et al., 2017; Raven, Fike, Gomes, et al., 2019; Gomez-Saez et al., 2021), and sinking marine particles in both sulfidic basins and anoxic (non-sulfidic) ODZs (Raven, Sessions, Adkins, et al., 2016; Raven et al., 2021). The sulfurization of OM in sinking marine particles could have a particularly large effect on fluxes in the marine carbon cycle because it impacts a relatively large and reactive pool of sinking biomass, where moderate changes in preservation efficiency can translate into substantial changes in the rates of sedimentary OM burial (Raven et al., 2018).

In this study, we investigate how sinking marine particles from the eastern tropical North Pacific ODZ respond to a brief exposure to environmentally relevant sulfidic conditions. The 48-hour duration of these experiments could be analogous to, for example, the experience of a large particle sinking through a polysulfide-rich chemocline in the water column. Previous sulfurization experiments that demonstrated rapid OM sulfurization generally used model compounds (Amrani and Aizenshtat, 2004b) or elevated temperatures, phase transfer agents, and/or elevated polysulfide concentrations that make them challenging to directly compare with modern marine environments (e.g., 50°C, 13 mM [poly]sulfide, 30 days) (Gelin et al., 1998; Kok, Rijpstra, et al., 2000; van Dongen et al., 2003). Here, we conduct two-day experiments with natural particle samples under environmental conditions (20°C, 0.5 mM [poly]sulfide), and use an expanded suite of X-ray spectroscopic techniques, to investigate how sulfidic conditions transform sinking marine particles.

2. Materials and Methods

2.1 Polysulfide solution preparation

Polysulfide solutions were prepared by combining 50 mg of natural-abundance S^0(s) (Sigma Aldrich, trace metal grade) and 1 mg of ^{34}S-labeled (≥98%) $^{34}S^0$(s) in O_2-free ultra-pure water with 1.25 mL of 400-mM sodium sulfide solution adjusted to pH 8 (with HCl). Solutions were equilibrated in the presence of this excess S^0(s) at 18˚C in the dark for >60 days before use, at which point S-isotope compositions in the aqueous phase were stable and fully equilibrated with solids. The total concentration of dissolved (poly)sulfide S in solution under these conditions was ~12 mM.

In a fully aqueous system, polysulfide speciation would be controlled primarily by pH and the relative abundances of sulfur and sulfide precursors. In the presence of excess S^0(s), however, the major species present in mixed polysulfide solutions are primarily a function of pH. At pH 8, experimental polysulfide solutions are largely composed of bisulfide anions and mid-chain-length polysulfides: $HS^- > S_5^{2-} > S_6^{2-} > S_4^{2-}$ (Rickard and Luther, 2007). Solid-phase S^0 was removed by in-line filtration during injection of the polysulfide solution into experiments.

2.2 Sampling site

Samples (IGSN: IEMRRETNP) were collected from the eastern tropical North Pacific ODZ in spring 2018 as part of cruise RR1807 on the R/V Roger Revelle. We deployed a surface-float-tethered particle trap with a 2-meter-diameter, 50-µm-mesh net (Van Mooy and Keil, 2015) at two sites: a relatively low particle flux site ('P2,' 200 km from the Mexican coast, 17.0°N x 107.0°W, ~3500 m water depth), and a relatively high particle flux site ('P1,' ~50 km from shore, 20.3°N x 106.1°W, ~1500 m water depth). This same population of samples was also used for radiosulfur measurements of microbial sulfate reduction rates and the identification of *in-situ* organic S formation (Raven et al., 2021). Particles were trapped at the depth of the secondary nitrite maximum (120-143 m at P1 and 147 m at P2) for approximately 48 hrs. After recovery, the 2-m-diameter net, which closed *in-situ* before recovery, was rinsed with filtered surface seawater to collect particles. Samples for this study (Table S1) include one sample from P2 ('F') and five samples from P1 ('A' through 'E'), all of which were collected from the 'net wash.' During processing, the

experimental sample from P2 was lost due to an unfortunate wind incident. Aliquots for controls ('A_C,' B_C,' etc.) were syringe-filtered in a N_2-filled glovebag onto pre-combusted, 0.7 μm (GF-F) glass fiber filters and immediately frozen under N_2 headspace at –20°C. Aliquots for polysulfide exposure experiments ('A_{Sx},', B_{Sx},' etc.) were transferred to 250-mL serum bottles and sparged with N_2. Each experiment received 10 mL of the 12-mM, filtered, ^{34}S-labeled, mixed polysulfide solution yielding a total reduced sulfur concentration in experiments of 0.52 mM. Bottles were incubated for 48 hrs at ~20°C in the dark. After incubation, 1-mL aliquots of seawater were filtered through GF-F filters into vials containing concentrated HCl to volatilize H_2S and then preserved with $BaCl_2$ for sulfate S-isotope analysis. Particle solids were collected anoxically onto pre-combusted GF-F filters and frozen under N_2 at –20°C.

2.3 Sample collection, handling, and processing

Particle samples were subdivided into three pools for analysis: extractable lipids (OM_{Lipid}), acid-soluble/volatile materials (OM_{Hyd}), and acid-resistant organics (OM_{Res}), as diagrammed in Figure S1. After filters were washed with N_2-sparged pH 7.8 tris buffer solution to remove inorganic sulfate and lyophilized, splits were set aside for 'whole particle' spectroscopy, and selected controls with sufficient particle material were split to allow elemental and isotopic analysis of 'whole particles' with minimal disruption. Remaining particles were microwave-extracted (CEM MARS-6) twice in 9:1 dichloromethane:methanol. Solvent extracts were concentrated under N_2 and exposed to activated Cu^0 for 12 hrs to remove elemental S. Lipid extract aliquots for XAS were dried onto quartz slides, and the remaining material was trapped onto washed and dried silica gel for elemental analysis. Splits of solvent-extracted particle filters were set aside for X-ray absorption spectroscopy and X-ray fluorescence mapping (XAS/XRF), and experimental samples with sufficient material were split for elemental analysis. Experimental particles were split after solvent extraction to ensure removal of reactant polysulfide before S quantification.

All solvent-extracted particles were subjected to acid-volatile sulfide (AVS) extraction with hot (~70°C) 6N hydrochloric acid under flowing N_2 (Rickard and Morse, 2005; Raven, Fike, Gomes, et al., 2019). In addition to volatilizing sulfides from FeS, this method solubilizes a large proportion of the

carbohydrates and proteins in OM (Hill, 1965). After AVS hydrolysis, remaining solids were washed in ultra-pure water and divided into splits for XAS and for elemental analysis.

2.4 EA-IRMS analysis

Carbon isotopes and S:N:C elemental ratios of lipid extracts and whole and AVS-extracted particles were analyzed at UCSB with an Elementar Vario Isotope Select elemental analyzer (EA), which includes a ramped-temperature column to improve SO_2 peak shape, coupled to a Nu Horizon isotope ratio mass spectrometer (IRMS). C-isotope data were internally standardized to CO_2 gas standards and calibrated to VPDB using the caffeine isotope standards USGS-61, -62, and -63. Reported uncertainties reflect long-term uncertainties for replicate sulfanilamide standards. Whole particle samples before acidification retain some seawater sulfate, as quantified by XAS (below); reported S:C ratios for 'whole particle' and 'solvent-extracted' OM were corrected (uncorrected data included in Table S2) to remove the proportional contributions from inorganic phases (sulfate and FeS) based on the relative abundances of these phases in XAS spectra. S-isotope values for dissolved sulfate at the end of the polysulfide exposure experiment and for the initial polysulfide spike were measured by EA–IRMS as barium sulfate and zinc sulfide, respectively. Samples contained WO_3 as a combustion aid, and S-isotope values were calibrated to VCDT using the isotope standards IAEA-S1, S2, S3, and S5. The $\delta^{34}S$ values for the ^{34}S-labeled polysulfide spike are estimates because they exceed the calibration range of these standards.

XAS/XRF analysis and data processing

The redox speciation and bonding environment of sulfur and iron in the filter-bound particles were analyzed at the Stanford Synchrotron Radiation Lightsourse (SSRL). Glass fiber filter pieces were adhered onto Saint Gobain M60 S-free polyester tape and covered in 5-μm-thick SPEX 3520 polypropylene XRF film. 'Bulk' sulfur K-edge spectra (500 μm^2 spot size) were collected on beam line 14–3 on whole particles, solvent-extracted particles, HCl-extracted particles, and lipid extracts, before and after copper exposure. Additionally, a micro-focused X-ray beam was used to map S and Fe species by rastering over selected mapping areas at specific energies (for sulfur: 2472.0, 2472.9, 2473.9, 2474.25, 2476.15, 2477.8, 2481.4,

191 2482.6, and 2486.0 eV; for iron: 7116.0, 7128.0, 7133.0, 7139.0, and 7147.0 eV) to create elemental and
192 chemical distribution maps. Full XAS spectra were collected from 2460 to 2540 eV (sulfur) or 6900 to 7500
193 eV (iron) at selected spots.

194 Sulfur data were collected at SSRL beam line 14–3, which is equipped with a Si(111) ($\Phi = 90$) double
195 crystal monochromator and calibrated to the thiol pre-edge peak of thiosulfate at 2472.02 eV. The S Kα
196 fluorescence line was measured with a Si Vortex Si drift detector (Hitachi) using Xspress3 pulse processing
197 electronics (Quantum Detectors). The X-ray beam was focused using an axially symmetric focusing mirror
198 (SIGRAY) to a size of 5 x 5 μm at a flux of ~8 x 10^{10} photons per second; maps were collected at a resolution
199 of 5 μm^2. Sulfur XAS spectra were processed in the SIXPACK (Webb, 2005; Webb, 2020) software
200 package using a K-edge E0 of 2473 and pre-edge and post-edge linear normalization ranges of –20 to –7
201 and 35 to 70 eV, respectively. Sulfur K-edge fitting standards are shown in Figure S2. Uncertainties
202 reported in Table S3 refer to the confidence in the linear combination fit calculated in SIXPACK. Iron data
203 were collected at SSRL beam line 2–3, a bending magnet workstation equipped with a Si(111) ($\Phi = 0$)
204 double crystal monochromator calibrated such that the first derivative of an Fe metal foil was set to 7112
205 eV. The beam line uses an axially symmetric focusing mirror (SIGRAY) to achieve a spot size of 5 x 5 μm
206 at a flux of ~5 x 10^8 photons per second at 7100 eV, and uses a similar fluorescence data collection system
207 as above with 14-3 to collect K-edge Fe spectra from 6900 to 7500 eV and elemental maps of Ca, P, Mn,
208 Ti, S, and other metals at 5-μm resolution. XRF maps from both beam lines were processed using the
209 MicroAnalysis Toolkit (SMAK; (Webb et al., 2011)). Sulfur XANES fitting used 3-pt blurred maps
210 (standard deviation 0.5) and a set of six standard spectra (FeS, methionine, glutathione disulfide, methionine
211 sulfoxide, cysteic acid / sulfonate, and sulfate ester, Fig. S2).

212

213 ## 3. Results

214 ### 3.1 EA–IRMS results

215 The carbon-isotope compositions of sinking particle materials are similar for samples from both
216 the high- and low-particle-flux sites (A–E and F, respectively; Fig. 1A and Table S2). Whole washed
217 particles before acidification, which may contain both organic C and calcium carbonate, have $\delta^{13}C$ values
218 between –26.0 and –23.7‰ (mean –24.6‰), while lipid extracts have relatively ^{13}C-depleted compositions
219 (Hayes, 2001) between –32.9 and –28.3‰ (mean –30.4‰). Accordingly, the $\delta^{13}C$ values for S_x-exposed,
220 solvent-extracted particles are higher (mean –22.0‰) than those for whole particle controls due to the
221 removal of ^{13}C-depleted lipids by solvent extraction (Fig. 1A). After both lipid extraction and strong
222 acidification (6N HCl, 70°C, 2 hrs), residual particle material (OM_{Res}) from both experiments and controls
223 has a $\delta^{13}C$ value between –27.4 and –25.0 (mean –25.7‰). There is no significant change in the C-isotope
224 composition of either OM_{Res} or OM_{Lipid} associated with S_x exposure.

225 The nitrogen contents of whole particles, lipids, and OM_{Res} primarily track the abundance of protein
226 in each pool (Fig. S3). Whole particles N:C ratios (8.9 – 15.3 mol%) are typical for protein-rich, primary
227 producer biomass that has experienced some degradation (16:117 = 13.7%; (L. Anderson and Sarmiento,
228 1994)), while lipid extracts have lower N:C ratios (0.6 – 3.8 mol%). Molar N:C ratios in OM_{Res} controls
229 are between 2.5 and 4.7 mol%. In some cases, S_x-exposed OM_{Res} contains significantly more N than OM_{Res}
230 controls, with N:C ratios of up to 7.8 mol% (sample D_{Sx}; Fig. S3).

231 Sulfur-isotope compositions of dissolved sulfate in experimental bottles are between 22.6‰ and
232 24.3‰, summarized in Table S2. Replicates of the polysulfide spike were trapped as zinc sulfide and thus
233 reflect thio sulfur (bisulfide and roughly half of polysulfide S); the effect of excluding zero-valent
234 polysulfide S is negligible in this case given the much larger uncertainties from standard extrapolation.
235 Spike $\delta^{34}S$ values average 342.2‰ (Table S3).

236 Particle S:C ratios (Fig. 1B) increase in response to S_x exposure, reflecting the addition of
237 (poly)sulfide S to particulate OM. In controls, the S:C ratio of organic materials in whole particles is 0.64–
238 0.74 mol% at high-flux site P1 and 1.3 mol% in one sample from low-flux site P2 (Table S2). OM_{Res} and
239 lipids have lower S:C ratios, averaging 0.3 mol% and 0.4 mol%, respectively. After sulfurization, organic

materials in whole and solvent-extracted particles from P1 have S:C ratios between 1.7 and 2.1 mol%, an approximately 2.8-fold increase over P1 controls. Similarly, average S_x-exposed OM_{Res} S:C ratios average 1.1% (range 0.5 – 1.7%), a roughly 3.3-fold increase over P1 controls. Lipid extract S:C ratios are variable among samples (0.1 – 1.1%) and do not differ systematically between controls and S_x-exposed samples.

3.2 Bulk Particle XAS Speciation

The redox speciation of sulfur in particles varies systematically among lipid, hydrolyzable, and hydrolysis-resistant materials, and these distributions are consistent across samples from both sites and all depths (Fig. 2). Broadly speaking, the organic S (OS) in whole (control) particles from the ETNP is approximately 60% oxidized (sulfonates and sulfate esters) and 40% reduced (sulfides, disulfides, and aromatics). Organic solvent extracts are predominantly (58–78%) sulfate esters with up to 16% sulfonates, and the remaining 3.2 – 16.1% of the lipid OS pool is reduced. Hot acidification (6N HCl, 70°, 2 hrs) removed approximately 85% of the total sulfur in the particles, which included most of the non-lipid oxidized OS as sub-equal pools of sulfate esters and sulfonates. A reduced OS component is also removed by acidification that is best fit as aromatic S. After acidification, residual solids (OM_{Res}) contain sulfur predominantly as sulfides and disulfides, with smaller amounts of aromatics and oxidized forms, as was previously reported for parallel experiments with this population of particles (Raven et al., 2021).

After exposure to polysulfides for ~48 hrs, the speciation of sulfur in all five of the particle samples from site P1 was transformed, as summarized on the right-hand side of Fig. 2. Compared to controls, S_x-exposed particles contain a larger proportion of reduced species (sulfides and disulfides) and iron sulfides. S_x-exposed whole particles contain some elemental sulfur derived from the polysulfide reactant solution that was subsequently removed by solvent extraction and copper exposure. Copper-treated lipids after polysulfide exposure contained nearly 50% reduced OS in addition to the sulfate esters and sulfonates observed in the OM_{Lipid} controls. Reduced OS in the S_x-exposed lipids is composed of sulfides and disulfides with some zero-valent S. Particle materials lost during acidification include iron sulfides (AVS)

and roughly sub-equal pools of reduced and oxidized OS (OM_{Hyd}). OS in OM_{Res}, on the other hand, is almost exclusively reduced (sulfides and disulfides). Oxidized OS thus makes a smaller contribution to total OS in the experimental particles than in corresponding controls.

3.3 Particle XRF Maps

To examine the spatial variability in particle OS speciation, we mapped particles at 5-to-7-μm resolution using X-ray fluorescence imaging. Figure 3 presents maps of sulfur speciation in whole, buffer-washed particles from site P1 at 123 m depth (sample 'A_C'). Sulfur was not detected in filter backgrounds. Organic sulfur speciation is spatially heterogeneous in control particles, with separate regions that are rich in reduced versus oxidized organic S. The abundance of reduced organic S at specific spots ranges from 20.5% (spot 8) to 72.5% (spot 2). Reduced organic S, including organic monosulfides, thiols, aromatics, and disulfides, appears as localized concentrations ranging from ≤ 7 μm (single pixel) to nearly 80 μm in diameter. Oxidized components (sulfonates and sulfate esters) are also found in discrete regions up to several hundred microns in size.

After exposure to polysulfides, particles accumulate organic monosulfides and disulfides (Fig. 4). The proportion of OS in reduced forms (sulfides, disulfides, and aromatics) ranges from 59.3 to 78.3% (Fig. 4A and Table S5), and the overall proportion of reduced S is higher, consistent with the results for bulk speciation (Fig. 2). Newly formed disulfides appear as irregularly sized splotches that are generally but not exclusively associated with other forms of organic S, especially organic monosulfides (e.g., spot 7). Regions that are relatively rich in oxidized OS are discrete and 100–200 μm in size, similar to those observed in controls. In contrast, iron monosulfides are found throughout sulfurized particle materials and do not generally accumulate as singular particulates. Despite its relatively low abundance, the presence of FeS in these samples is confirmed by the characteristic pre-edge peak near 2470 eV in the XAS spectra from Fig.

4A (shown in Fig. S4). Gypsum (calcium sulfate) was also detected as an individual 25-μm-diameter particulate (spot 6).

Most of the iron on the particle filters is present as discrete, 15–40 μm particulates (Fig. 5). Prior to polysulfide exposure, iron oxyhydroxides are scattered throughout the samples and are not spatially associated with either carbonates or organic matter (P or S). After polysulfide exposure, some of these discrete iron particulates remain (e.g., C_{Sx}, Fig. 5), but iron also accumulates throughout the particles as a low, uniform abundance phase that is broadly co-located with sulfur. Based on XAS spectra in Fig. 4, at least some of this material is FeS (e.g., mackinawite).

4. Discussion

4.1 Controls: Organic sulfur speciation in sinking marine particles

Sulfur is a major component of biomass. Molar S:C ratios for marine biomass are typically 0.5–1‰, although they can be lower in woody plants and higher in some S-cycling microorganisms (Matrai and Eppley, 1989; Chen et al., 1996). The speciation of organic sulfur in particles (Fig. 2) reflects the contributions of various compound classes to functionally defined categories of OM, as well as any subsequent transformations of that OM due to enzymatic degradation, condensation, oxidation, and/or sulfurization.

Sinking particles from the ETNP ODZ contain the full suite of reduced and oxidized OS moieties that have been previously described for proteins, lipids, and carbohydrates. A large proportion (42–65%) of the assimilatory S in microplankton is typically found as proteins and polypeptides (Cuhel et al., 1982), specifically the amino acids cysteine, which is a thiol, and methionine, which is an organic monosulfide. Cysteine and methionine are highly susceptible to oxidation, both in the environment and during laboratory handling, which will produce sulfoxide (Vogt, 1995) and/or sulfonate (Phillips et al., 2021). The AVS hydrolysis method used here to isolate OM_{Res} is less intense (shorter duration and lower temperature) but

312 otherwise similar to some early methods for protein hydrolysis (e.g., 24 hrs, 110°, 6N HCl) (Hill, 1965).
313 Therefore, AVS hydrolysis is likely to solubilize many proteins in our particles, which is supported by the
314 drop in molar N:C ratios from whole particles (averaging 11.6%) to OM_{Res} (averaging 4.5%; Fig. S1).
315 However, we find that most of the OS in the OM_{Hyd} pool is relatively oxidized (Fig. 2), suggesting that
316 cysteine and methionine are not major contributors to OM_{Hyd}. (We calculate speciation by comparing solids
317 before and after hydrolysis, so the lack of reduced S in OM_{Hyd} is not caused by amino acid oxidation during
318 hydrolysis.) Instead, the reduced OS species in OM_{Hyd} are best fit as aromatic, and the main peak in their
319 XAS spectra at ~2473.5 eV is resolvably shifted relative to cysteine and methionine. Although aromatic
320 OS compounds have been attributed to rapid OM sulfurization in a few cases (i.e., phytol thiophene,
321 (LaLonde et al., 1987; Raven, Sessions, Adkins, et al., 2016)), aromatic OS is generally rare in modern
322 samples, and we do not observe aromatic OS formation during polysulfide experiments (below). The
323 immediate provenance of apparent aromatic OS in OM_{Hyd} from untreated particles is thus not yet known.
324 Rather than appearing in OM_{Hyd}, organic monosulfides and thiols account for ~80% of the S in OM_{Res} from
325 control particles. These functional groups are localized in cell-sized (≤ 20 um) structures, which suggests
326 they may be proteinaceous (Raven et al., 2021). In addition to amino acids, these structures contain organic
327 disulfides that may reflect amino acid dimers, like cystine. Finally, even in these unamended 'control'
328 samples, we expect to have at least trace contributions of sulfides and/or disulfides to OM_{Res} from *in-situ*
329 OM sulfurization, as we observed using radiolabels in Raven et al. (2021).

330 Oxidized OS compounds comprise the majority of total OS in lipids, OM_{Hyd}, and whole particles.
331 Lipid extracts are particularly rich in sulfate esters, which could represent sulfated hormones (e.g.,
332 cholesterol sulfate) and/or various sulfoglycolipids common in animals (Benson et al., 1959; R. Anderson
333 et al., 1978; Ishizuka, 1997). Lipids also contain sulfonates, which could reflect contributions from common
334 S-bearing lipids like sulfoquinovosyl diacylglycerides (SQDGs). In OM_{Hyd}, carbohydrates appear to be
335 major sources of oxidized OS, especially sulfate esters (Fig. 2). Exudates from macrophytoplankton can be
336 major sources of such sulfate-ester-bearing polysaccharides (Ramus and Groves, 1974; Percival et al.,

1980) and are likely to be particularly important here, because these extracellular polysaccharides, which can be produced in vast quantities by diatoms, are thought to contribute directly to the formation of large, sinking particles (Alldredge and Silver, 1988; La Rocha and Passow, 2007; Arnosti et al., 2021; Vidal-Melgosa et al., 2021). Hydrolyzable sulfate esters are also frequently localized in irregularly sized particles (Fig. 3) that could represent detritus from plants and animals and/or sulfated polysaccharides from algal exudates (Vidal-Melgosa et al., 2021). Overall, these XAS data underscore the substantial contributions of oxidized OS species to lipids and carbohydrates in marine particles, which can be clearly distinguished from amino acids and the products of abiotic OM sulfurization.

4.2 Experiments: Organic products of particle sulfurization reactions

In a separate study (Raven et al., 2021), we used radiolabeled sulfate to identify organic S formation in sinking marine particles under anoxic, sulfide-limited, ODZ-like conditions. Here, we investigate how this same population of particles would be transformed by short-term exposure to more strongly reducing, sulfidic conditions. Polysulfide concentrations in our experiments (~0.5 mM) are equivalent to or slightly higher than reported concentrations in a range of modern environments: the Great Salt Marsh (Boulegue et al., 1982; Luther et al., 1986), sulfidic lakes like Mahoney Lake (Overmann et al., 1996) and Fayetteville Green Lake (Zerkle et al., 2010), and the Black Sea (Holmkvist et al., 2011). Polysulfide concentrations can be even higher in specific environments like microbial mats, where up to 100s of mM polysulfides have been reported (Findlay, 2016). Conditions in experimental bottles therefore coarsely reproduce the experience of particles in certain modern and ancient Earth environments.

Experiments with particles and (poly)sulfide generated organic S in the proto-kerogen, hydrolysable, and lipid pools. Based on XAS fits, organic S accounts for the majority (67 to 82%) of the newly formed non-lipid particle solids (Fig. 6); inorganic products (iron sulfides) are discussed in Section 4.3, below. The initial molar S:C ratios in total particle OM from high-flux site P1 average 0.69% (range 0.64 – 0.74%), and these ratios increase after 48 hours of polysulfide exposure to an average of 1.9% (range

362 1.7 – 2.1%). OM S:C ratios are somewhat lower in the OM_{Res} pool, averaging 0.33% before, and 1.1% after,
363 polysulfide exposure (Fig. 1B). These S:C ratios are similar to those found in OM_{Res} in sediments from O_2-
364 limited continental margin sediments, including the Santa Barbara Basin (OM S:C ratios average 2.1 mol%
365 in the upper 50 cm; (Raven, Sessions, Fischer, et al., 2016)), the Peru Margin (0.5 – 2.3% in the upper meter
366 of sediments; (Mossman et al., 1991; Suits and Arthur, 2000), and the Namibian Margin (OM S:C ratios
367 average 2.3% for all data; (Dale et al., 2009)). But, sulfurized particle S:C ratios remain below those
368 observed for OM in sulfidic basins like the Cariaco Basin (~4 mol%; (Werne et al., 2003)). It is likely that
369 longer–term exposure to polysulfides would further increase the S content of particle OM, eventually
370 reaching 'saturation' or full sulfurization of the functional groups that are reactive on the timescale of
371 interest, as modified by other environmental factors (Amrani et al., 2007). The change in particle S:C ratios
372 as a result of sulfurization indicates that organic precursor molecules contained at least that density of
373 rapidly sulfurizable functional groups (aldehydes, ketones, certain re-arrangable alcohols, and conjugated
374 double bonds (Kutuzov et al., 2020)). Primary biogenic molecules can also gain sulfide-reactive functional
375 groups like carbonyls through photochemical reactions in the euphotic zone (Amrani and Aizenschtat
376 2004c).

377 The short duration of these 48–hour experiments makes it possible to investigate potential OM
378 preservation processes on the same timescale as particle OM breakdown and remineralization. Typical
379 sinking particle OM remineralization rates are ~12% per day (Iversen and Ploug, 2013; Cavan et al., 2017),
380 which means that reactions that transform particle OM within days are particularly important for impacting
381 the extent of OM remineralization in sinking particles and, by extension, carbon fluxes to the sediments.
382 Additionally, the large changes in organic S chemistry observed within 48 hours in these experiments
383 demonstrate that even intermittently sulfidic conditions – on the timescale of hours to days – can have a
384 dramatic effect on the composition of particulate OM.

385 The initial products of particle sulfurization are primarily organic monosulfides and disulfides (Fig.
386 6). Although three of the five sulfurized samples also contained more sulfonates or sulfate esters than their

387 respective controls, this likely represents heterogeneity in the distribution of assimilatory OS particles
388 among control and experiment filter aliquots. In Figure 6, the speciation of newly formed materials is
389 calculated by assuming that sulfurization adds new sulfur to an unchanging pool of biogenic OS, as
390 measured in the control sample. The calculated, newly formed OS is very similar to the overall speciation
391 of S_x-exposed OM_{Res} (Fig. 2) and is consistent with observations from the sulfurization of standard
392 compounds under conditions similar to those investigated here (Amrani and Aizenshtat, 2004b). In those
393 experiments, α, β-unsaturated aldehydes, including the chlorophyll-derived C_{20} isoprenoid phytenal, were
394 exposed to a polysulfide solution and the products were identified as disulfide-bridged oligo-polymers.
395 Nucleophilic polysulfides attacked the conjugated double bond rapidly (within hours) and the carbonyl
396 group more slowly, leading to carbon skeletons cross-linked by two or more S_x (e.g., polysulfide) bridges
397 within days to weeks (Amrani and Aizenshtat, 2004b). Similar mechanisms could explain the observed
398 rapid formation of organic sulfides, disulfides, and polysulfides ($S_{x\geq3}$) during the sulfurization of sinking
399 marine particles.

400 Newly formed organic disulfides appear within certain particle regions that range from 30 to 300
401 μm in diameter (Fig. 4). These 'strongly sulfurized' regions often envelop clusters of small (single-pixel; ≤
402 5 μm), sulfide-rich particulates that are interpreted as cells. And, they are also frequently associated with
403 the larger (20–200 μm), sulfate-ester-rich irregular particles that may represent concentrations of
404 polysaccharide exudates or contributions from plant or animal detritus. These spatial relationships suggest
405 that sulfurization affects a ubiquitous particle component that naturally contains a lower concentration of
406 organic S than other forms of biomass. Exopolymeric substances (EPS) are a leading candidate for this
407 component. EPS is a loosely-defined blend of polysaccharides, proteins, nucleic acids, and lipids, with
408 carboxylate, amine, hydroxyl, sulfate, and phosphate functional groups (Alvarado Quiroz et al., 2006;
409 Braissant et al., 2007). EPS is an important contributor to the formation of large, sinking particles, building
410 particle size and density by binding organic and inorganic solid materials together (Alldredge and Silver,

411 1988; Passow et al., 1994; Bhaskar and Bhosle, 2005). The abundance of EPS in large sinking particles
412 may make these organic materials particularly susceptible to rapid sulfurization.

413 XAS results strongly indicate that lipids sulfurize alongside non-lipid OM over 48 hours of
414 polysulfide exposure, despite the lack of consistent trends in lipid S:C ratios. Variable lipid S:C ratios
415 among samples, both before and after sulfurization, most likely reflect the heterogeneous distributions of
416 specific particle components (e.g., animal detritus; Ishizuka 1997) that are key sources of sulfated lipids.
417 Sulfurization may also reduce the solubility of lipid molecules and transfer them functionally to the OM_{Res}
418 pool, although here this process was insufficient to significantly lower the C-isotope composition of OM_{Res}
419 (Fig. 1A). Newly formed lipid OS is compositionally similar to newly formed non-lipid OS, with varying
420 proportions of organic sulfides, disulfides, and oxidized species. Sulfurized lipids also contain zero-valent
421 S that may represent the S^0 atoms in S_3 and longer organic polysulfides, which may therefore be more
422 important in lipids than for other organic precursors (Fig. 6). Rapid lipid sulfurization has been documented
423 for specific lipid molecules both experimentally and in the environment (Van Mooy et al., 2002; Amrani
424 and Aizenshtat, 2004b; Raven, Sessions, Adkins, et al., 2016), while other specific lipids are known to
425 sulfurize over thousands of years (Kok, Rijpstra, et al., 2000; Werne et al., 2000). The observed changes in
426 the speciation of total extractable lipid OS help to scale up these compound-specific observations and
427 indicate that rapid sulfurization can impact a substantial proportion of the bulk sedimentary lipid pool.

428

429 ***4.3 Experiments: Competitive sinks for polysulfides***

430 Dissolved sulfide (H_2S/HS^-) has many possible reaction pathways in real, complex marine
431 particles. In addition to reactions with OM, both microbial sulfide oxidation and iron sulfidization can occur
432 rapidly, generating inorganic sulfur species with redox states ranging from S^0 to sulfate, and iron sulfides,
433 respectively.

We use the appearance of ^{34}S-labeled sulfate to estimate the scale of polysulfide oxidation during the 48-hour experiment. The $\delta^{34}S$ value of seawater sulfate increased during the experiment to values between 22.6 ± 0.4‰ and 24.3 ± 0.4‰, a significant change from initial sulfate at ~21‰. Given a 28 mM concentration of seawater sulfate, these values indicate the addition of between 140 and 295 μM sulfate with a $\delta^{34}S$ value matching the polysulfide spike (~342‰), which represents a substantial proportion (27 – 57%) of the 520 μM polysulfide solution originally added to each experiment. Some of this (poly)sulfide oxidation may have occurred abiotically through reaction with any dissolved O_2 that was introduced during on-deck handling of these 'net wash' samples and incompletely removed during gentle sparging with N_2. However, even dissolved O_2 concentrations of as much as 10 μM would account for only a few percent (~5 μM) of this sulfate production. Instead, most (poly)sulfide oxidation likely occurred through microbial processes, which can be highly efficient at drawing down limiting sulfide concentrations, generating a tightly coupled and often cryptic sulfur cycle in sediments (Canfield et al., 1992; Jorgensen, 2019) and the water column (Canfield et al., 2010; Johnston et al., 2014). Given ETNP ODZ conditions, nitrate is likely to be a main oxidant powering sulfide oxidation in the dark (Devol et al., 2019). Net rates of (poly)sulfide oxidation in our experimental bottles were ~100 μM/day, which is similar to sulfide oxidation rates reported for very different environments like shallow marine sediments (Findlay et al., 2020). Notably, OM sulfurization occurs in particles despite this active competition for (poly)sulfide from oxidative sinks. Although this oxidative cycle likely generated some quantity of more oxidized inorganic sulfur species (e.g. thiosulfate), the key reactant for OM sulfurization is still most likely polysulfide because this matches the redox state of the newly formed organic S.

Another important sink for (poly)sulfide in particles is the formation of iron sulfides. The initial product of the reaction between Fe^{2+} and S^{2-} is an iron monosulfide (e.g., FeS(aq), mackinawite). Given unlimiting sulfide, the rate of this reaction depends on the availability of Fe^{2+}, which is typically sourced from the reduction of Fe(III)-oxyhydroxides and other reactive Fe(III) species. Marine particles from ODZs frequently contain Fe^{3+} in the form of iron(III) oxyhydroxides, which appear to be actively recycled between

459 dissolved Fe^{2+} and particulate Fe(III) minerals (Resing et al., 2015; Heller et al., 2017). We observe similar
460 iron species in our control particle samples; the first-derivative X-ray spectra for iron in these particulates
461 (Fig. 5) have similar spectral features to Fe(III) oxyhydroxide standards. Before S_x exposure, these iron
462 oxyhydroxides are found in discrete, 10–50 μm-diameter particles with a broadly round morphology. These
463 iron-bearing particulates are found throughout the mapped samples (A, B, and C) and are not spatially
464 associated with calcium, phosphorus, or total sulfur.

465 After 48 hours of exposure to polysulfides, iron sulfides (FeS) form that have a distinctly different
466 distribution than their Fe(III) precursors. FeS does not appear as discrete, resolvable particles and instead
467 accumulates to low, uniform concentrations throughout the same, ~200-μm-scale particle regions that
468 accumulate organic S (Fig. 5). Although Fe(III) particulates do not appear to be local FeS formation
469 hotspots, they must be the source of iron for FeS formation because dissolved Fe^{2+} concentrations in the
470 ETNP ODZ are only ~2 nM (*Bolster et al., under review GCA*) and iron backgrounds in the EPS from
471 controls are low (Fig. 5). FeS formation therefore most likely proceeded through the reductive dissolution
472 of Fe(III) oxyhydroxides by sulfide to dissolved Fe^{2+}, which was subsequently precipitated from solution
473 as FeS. Iron-cycling microbes may also play a role in the generation of dissolved Fe^{2+}. Although greater
474 temporal resolution is needed to evaluate the kinetic competition between sulfurizable organic moieties and
475 Fe^{2+} for sulfide, the concurrent and co-located formation of FeS and OS within 48 hrs illustrates the tightly
476 coupled formation of both inorganic and organic sulfur phases in sedimentary systems.

477 Sulfide-derived organic S has been seen to accumulate prior to the complete consumption of iron
478 oxyhydroxides across diverse marine and lacustrine environments (Francois, 1987; Hartgers et al., 1997;
479 Urban et al., 1999; Filley et al., 2002; van Dongen et al., 2003; Dale et al., 2009; Raven, Sessions, Fischer,
480 et al., 2016). At the same time, environments with abundant reactive iron and active iron cycling can
481 suppress the formation of organic and inorganic S (Shawar et al., 2018). The relative rates of formation for
482 organic and inorganic S are complex and will depend on the identities and morphologies of organic and
483 inorganic precursors, local geochemical conditions, and spatial relationships between sulfide sources and

484 potential sinks. It is clear, however, that organic S has the potential to preserve S-isotope signals that reflect
485 a water column, particle-hosted sulfur cycle. We speculate that relatively rapid microbial sulfate reduction
486 with fresh, particle OM may generate smaller S-isotope fractionations between sulfate and sulfide and
487 therefore more ^{34}S-enriched dissolved sulfide, OS, and FeS than equivalent metabolisms in near-surface
488 sediments. The S-isotope composition of sulfide in particles may also be impacted by closed-system
489 processes within diffusively-limited particle microenvironments, and by the activity of tightly coupled
490 microbial metabolisms in addition to microbial sulfate reduction. In all of these cases, OS δ^{34}S values can
491 be influenced by processes outside of a traditional, one-dimensional sedimentary diagenetic framework.

492

493 ***4.4 Implications for the long-term preservation of sulfurized OM***

494 Because particle OM can sulfurize rapidly, even brief periods of sulfidic conditions in the
495 environment have the potential to transform the chemical structure of sinking particulate OM and impact
496 its lability. OM sulfurization is thus capable of transforming OM in temporally dynamic systems with only
497 intermittently sulfidic conditions, ranging from tidally and photosynthetically cyclic systems like microbial
498 mats and inter-tidal habitats to environments with strong seasonal upwelling. In sulfidic lakes and basins,
499 sinking particles that encounter a layer of polysulfide-rich water near the O_2–H_2S chemocline (Overmann
500 et al., 1996; Li et al., 2008) are likely to carry a signal of rapid OM sulfurization reactions to underlying
501 sediments, similar to interpretations of pyrite δ^{34}S values from the Black Sea and Cariaco Basin (Lyons,
502 1997; Lyons et al., 2003). The isotopic composition and speciation of organic sulfur preserved in sediments
503 will in part reflect rapid reactions in polysulfide-rich hotspots.

504 Prior to long-term burial, however, the initial products of particle sulfurization may experience
505 additional condensation reactions, enzymatic attack, and changing environmental conditions that could
506 further alter their chemistry. Organic di- and poly-sulfides may be particularly susceptible to isotope
507 exchange with inorganic polysulfides and chemical maturation – the rearrangement of bonds to more
508 energetically stable forms during sedimentary diagenesis (Canfield et al., 1998; Amrani et al., 2006).

Organic polysulfide maturation would decrease the proportion of organic polysulfides and disulfides over time and increase the abundance of monosulfidic or aromatic moieties (Kohnen et al., 1991; Amrani et al., 2006), which are more common in ancient deposits. S-isotope exchange between organic and inorganic polysulfides could also help explain puzzling S-isotope distributions among sedimentary phases in shallow anoxic sediments (i.e., (Dale et al., 2009; Raven, Sessions, Fischer, et al., 2016)). Here, our experiments with relatively high concentration of polysulfides strongly favor the formation of organic di- and poly-sulfides relative to reactions with sulfide (Kohnen et al., 1989). As a result, OM contains an average of 52.4% disulfides (range 46.8 to 67.4%; Fig. 6, excluding FeS), which is significantly higher than control OM_{Res} from untreated particles, which averages 31.3% (range 23.4 to 47.7%) disulfides, or than kerogens from 100-million-year-old black shales, which have a maximum reported disulfide content of ~28% (Raven, Fike, Bradley, et al., 2019; Raven et al., 2021). Depending on the scale and timing of organic polysulfide exchange and maturation in the environment, the $\delta^{34}S$ values recorded in sedimentary OM may partially reflect later generations of environmental (poly)sulfide rather than the S-isotope composition of the (poly)sulfide that initially drove OM sulfurization. Further work is needed to better understand the stability of OM $\delta^{34}S$ values during very early diagenesis and the preservation potential of rapidly-formed organic polysulfides. Organic polysulfide maturation could also serve as a source of sulfur to other sedimentary reactions, including the conversion of iron monosulfides to pyrite, S^0 disproportionation, or gradual lipid sulfurization.

OM sulfurization in sinking marine particles has substantial implications for the carbon cycle, both in response to anthropogenic climate change and during periods of Earth history with relatively widespread sulfidic conditions. In the modern ocean, sinking particle sulfurization could help explain the observation that sediments below a water column ODZ can have higher carbon contents than those under water columns without a strong O_2 minimum, even when bottom water is oxygenated (Lückge et al., 1996; Devol and Hartnett, 2001; B. Van Mooy et al., 2002; Keil et al., 2016). Due to the potential for rapid OM sulfurization in the water column, the ongoing expansion of ODZs (Schmidtko et al., 2017) may increase OM burial in

even deep-water, O_2-exposed sediments. OM burial during Ocean Anoxic Event 2 (~94 Mya) was also likely enhanced due to water column particle sulfurization, drawing down atmospheric CO_2 and impacting climate (Sinninghe Damsté and Köster, 1998; Hülse et al., 2019; Raven, Fike, Bradley, et al., 2019). On even longer timescales, there is widespread evidence for locally sulfidic conditions at intermediate water depths throughout the Proterozoic (Lyons et al., 2014; van de Velde et al., 2020). OM sulfurization may have influenced the efficiency of carbon burial throughout this period, modifying the organic carbon burial processes that contributed to the oxygenation of the surface Earth. On all of these timescales, particle OM sulfurization in the water column is a powerful lever connecting changes in local redox state to substantial transformations in the pool of OM delivered to, and preserved in, marine sediments.

5. Conclusions

Sinking, OM-rich marine particles are transformed by reactions with polysulfides within 48 hours. Organic materials in the acid-soluble, acid-resistant, and lipid pools can all sulfurize on this timescale. Iron monosulfides (FeS) also form concurrently, prior to the complete consumption of Fe(III) minerals, which indicates that organic matter and iron minerals can be competitive sinks for (poly)sulfide over short (day) timescales. Both organic S and FeS phases appear within regions of particles that are suggestive of extracellular polymeric substances (EPS), which may be particularly important substrates for sinking particle sulfurization. Rapid particle-hosted OM sulfurization has the potential to enhance total organic carbon burial in sediments and to help explain why marine sediments in sulfidic environments often preserve abundant OM.

The initial products of particle OM sulfurization are primarily organic monosulfides and disulfides. Subsequent transformations of this sulfurized OM during sedimentation and early diagenesis could further transform the speciation and/or isotopic composition of organic S. In ancient deposits, the S-isotope compositions of organic S and iron sulfides will depend on the availability and speciation of iron and organic reactants during their formation – potentially in the water column – as well as these later reactions.

Acknowledgements

This work was made possible through the support and generosity of A. Devol, G. Rocap, J. Neibauer, and M. Duffy at the University of Washington; D. Fike at Washington University in St. Louis; and V. Orphan and S. Connon at Caltech. Special thanks are also owed to M. O'Beirne (University of Pittsburgh) and the full science party and crew of the R/V Roger Revelle (RR1805). The manuscript was greatly improved by input from B. Toner and an anonymous reviewer. Financial support was provided under NSF Dimensions of Biodiversity award no. 1542240 (to R.G.K.) and the Agouron Institute Geobiology Postdoctoral Fellowship (to M.R.R.). Use of the Stanford Synchrotron Radiation Lightsource, SLAC National Accelerator Laboratory (proposal 5359) is supported by the U.S. Department of Energy, Office of Science, Office of Basic Energy Sciences under contract no. DE-AC02-76SF00515. The SSRL Structural Molecular Biology Program is supported by the DOE Office of Biological and Environmental Research and by the National Institutes of Health, National Institute of General Medical Sciences (P30GM133894). The contents of this publication are solely the responsibility of the authors and do not necessarily represent the official views of NIGMS or NIH.

Open Research / Data Availability

All of the processed data used in this manuscript are presented in the main text and supporting information. Data files are also archived on FigShare (10.6084/m9.figshare.16550790).

References

Alldredge A. L. and Silver M. W. (1988) Characteristics, dynamics and significance of marine snow. *Progress in Oceanography* **20**, 41–82.

Alvarado Quiroz N. G., Hung C.-C. and Santschi P. H. (2006) Binding of thorium(IV) to carboxylate, phosphate and sulfate functional groups from marine exopolymeric substances (EPS). *Marine Chemistry* **100**, 337–353.

Amrani A. and Aizenshtat Z. (2004a) Mechanisms of sulfur introduction chemically controlled: δ34S imprint. *Organic Geochemistry* **35**, 1319–1336.

Amrani A. and Aizenshtat Z. (2004b) Reaction of polysulfide anions with α, β unsaturated isoprenoid aldehydes in aquatic media: simulation of oceanic conditions. **35**, 909–921.

Amrani, A., & Aizenshtat, A. (2004c). Photosensitized oxidation of naturally occurring isoprenoid allyl alcohols as a possible pathway for their transformation to thiophenes in sulfur rich …. Organic Geochemistry, 35, 693–712.

Amrani, A., Said-Ahamed, W., Lewan, M., & Aizenshtat, Z. (2006). Experiments on d34S mixing between organic and inorganic sulfur species during thermal maturation. Geochimica Et Cosmochimica Acta, 70, 5146–5161.

Amrani A., Turner J. W., Ma Q., Tang Y. and Hatcher P. G. (2007) Formation of sulfur and nitrogen cross-linked macromolecules under aqueous conditions. *Geochimica et Cosmochimica Acta* **71**, 4141–4160.

Anderson L. and Sarmiento J. L. (1994) Redfield ratios of remineralization determined by nutrient data analysis. *Global Biogeochemical Cycles* **8**, 65–80.

Anderson R., Kates M. and Volcani B. E. (1978) Identification of the sulfolipids in the non-photosynthetic diatom Nitzschia alba. *Marine and Petroleum Geology* **528**, 89–106.

Arnarson T. S. and Keil R. G. (2007) Changes in organic matter–mineral interactions for marine sediments with varying oxygen exposure times. *Geochimica et Cosmochimica Acta* **71**, 3545–3556.

Arndt S., Jorgensen B. B., LaRowe D. E., Middelburg J. J., Pancost R. D. and Regnier P. (2013) Quantifying the degradation of organic matter in marine sediments: A review and synthesis. *Earth Science Reviews* **123**, 53–86.

Arnosti C., Wietz M., Brinkhoff T., Hehemann J. H., Probandt D., Zeugner L. and Amann R. (2021) The Biogeochemistry of Marine Polysaccharides: Sources, Inventories, and Bacterial Drivers of the Carbohydrate Cycle. *Annu. Rev. Mar. Sci.* **13**, 81–108.

Arthur M. A., Dean W. E. and Pratt L. M. (1988) Geochemical and climatic effects of increased marine organic carbon burial at the Cenomanian/Turonian boundary.

Benson A. A., Daniel H. and Wiser R. (1959) a Sulfolipid in Plants. In *Proceedings of the National Academy of Sciences of the United States of America.* **45**, 1582–1587.

Bhaskar P. V. and Bhosle N. (2005) Microbial extracellular polymeric substances in marine biogeochemical processes. *Journal of Paleontology* **88**, 45–53.

Bianchi T. S., Cui X., Blair N. E., Burdige D. J., Eglinton T. I. and Galy V. (2018) Centers of organic carbon burial and oxidation at the land-ocean interface. *Organic Geochemistry* **115**, 138–155.

Boulegue J., Lord C. J. III and Church T. M. (1982) Sulfur speciation and associated trace metals (Fe, Cu) in the pore waters of Great Marsh, Delaware. *Marine and Petroleum Geology* **46**, 453–464.

Boussafir M. and Lallier-Verges E. (1997) Accumulation of organic matter in the Kimmeridge Clay Formation (KCF): an update fossilisation model for marine petroleum source-rocks. *Marine and Petroleum Geology* **14**, 75–83.

Boyd P. W., Claustre H., Lévy M., Siegel D. A. and Weber T. (2019) Multi-faceted particle pumps drive carbon sequestration in the ocean. *Nature Publishing Group* **568**, 1–9.

Boye K., Noël V., Tfaily M. M., Bone S. E., Williams K. H., Bargar J. R. and Fendorf S. (2017) Thermodynamically controlled preservation of organic carbon in floodplains. *Nature Geosci* **10**, 415–419.

Braissant O., Decho A. W., Dupraz C., Glunk C., Przekop K. M. and Visscher P. T. (2007) Exopolymeric substances of sulfate-reducing bacteria: Interactions with calcium at alkaline pH and implication for formation of carbonate minerals. *Geobiology* **5**, 401–411.

Breitburg D., Levin L. A., Oschlies A., Grégoire M., Chavez F. P., Conley D. J., Garçon V., Gilbert D., Gutiérrez D., Isensee K., Jacinto G. S., Limburg K. E., Montes I., Naqvi S. W. A., Pitcher G. C., Rabalais N. N., Roman M. R., Rose K. A., Seibel B. A., Telszewski M., Yasuhara M. and Zhang J. (2018) Declining oxygen in the global ocean and coastal waters. **359**, eaam7240–13.

Canfield D. E., Boudreau B. P., Mucci A. and Gundersen J. K. (1998) The early diagenetic formation of organic sulfur in the sediments of Mangrove Lake, Bermuda. *Marine and Petroleum Geology* **62**, 767–781.

Canfield D. E., Raiswell R. and Bottrell S. H. (1992) The reactivity of sedimentary iron minerals toward sulfide. *American Journal of Science* **292**, 659–683.

Canfield D. E., Stewart F. J., Thamdrup B., De Brabandere L., Dalsgaard T., Delong E. F., Revsbech N. P. and Ulloa O. (2010) A Cryptic Sulfur Cycle in Oxygen-Minimum-Zone Waters off the Chilean Coast. *Science* **330**, 1375–1378.

Cavan E. L., Trimmer M., Shelley F. and Sanders R. (2017) Remineralization of particulate organic carbon in an ocean oxygen minimum zone. *Nature Communications* **8**, 2077–9.

Chen C., Lin C. M., Huang B. T., Chemistry L. C. M.1996 (1996) Stoichiometry of carbon, hydrogen, nitrogen, sulfur and oxygen in the particulate matter of the western North Pacific marginal seas. *Marine and Petroleum Geology* **54**, 179–190.

Cuhel R. L., Taylor C. D. and Jannasch H. W. (1982) Assimilatory Sulfur Metabolism in Marine Microorganisms: Sulfur Metabolism, Protein Synthesis, and Growth of Alteromonas luteo-violaceus and Pseudomonas halodurans During Perturbed Batch Growth. *Appl. Environ. Microbiol.* **43**, 151–159.

Dale A. W., Bruchert V., Alperin M. and Regnier P. (2009) An integrated sulfur isotope model for Namibian shelf sediments. *Geochimica et Cosmochimica Acta* **73**, 1924–1944.

Deutsch C., Brix H., Ito T., Frenzel H. and Thompson L. (2011) Climate-Forced Variability of Ocean Hypoxia. *Science* **333**, 336–341.

Devol A. and Hartnett H. E. (2001) Role of the oxygen-deficient zone in transfer of organic carbon to the deep ocean. *Limnology and Oceanography* **46**, 1684–1690.

Devol A. H., Keil R., Rocap, G. Haskins C., "CTD bottle data for all CTD casts during R/V Roger Revelle RR1804, RR1805 cruises in the Eastern Tropical North Pacific Ocean, from March to April 2018" (2019); www.bco-dmo.org/dataset/ 779185/data.

Dunne J. P., Sarmiento J. L. and Gnanadesikan A. (2007) A synthesis of global particle export from the surface ocean and cycling through the ocean interior and on the seafloor. *Global Biogeochemical Cycles* **21**, GB4006.

Filley T., Freeman K., Wilkin R. and Hatcher P. (2002) Biogeochemical controls on reaction of sedimentary organic matter and aqueous sulfides in Holocene sediments of Mud Lake, Florida. *Geochimica et Cosmochimica Acta* **66**, 937–954.

Findlay A. J. (2016) Microbial impact on polysulfide dynamics in the environment ed. R. Boden. *FEMS Microbiology Letters* **363**, fnw103–12.

Findlay A. J., Pellerin A., Laufer K. and Jorgensen B. B. (2020) Quantification of sulphide oxidation rates in marine sediment. *Geochimica et Cosmochimica Acta*, **280**, 441-452.

Francois R. (1987) A study of sulphur enrichment in the humic fraction of marine sediments during early diagenesis. *Geochimica et Cosmochimica Acta* **51**, 17–27.

Froelich P. N., Klinkhammer G. P., Bender M. L., Luedtke N. A., Heath G. R., Cullen D. and Dauphin P. (1979) Early oxidation of organic matter in pelagic sediments of the eastern equatorial Atlantic: suboxic diagenesis. *Geochimica et Cosmochimica Acta* **43**, 1075–1090.

Gelin F., Kok M. D., De Leeuw J. W. and Damsté J. S. S. (1998) Laboratory sulfurisation of the marine microalga Nannochloropsis salina. **29**, 1837–1848.

Gomez-Saez G. V., Niggemann J., Dittmar T., Pohlabeln A. M., Lang S. Q., Noowong A., Pichler T., Wörmer L. and Bühring S. I. (2016) Molecular evidence for abiotic sulfurization of dissolved organic matter in marine shallow hydrothermal systems. *Geochimica et Cosmochimica Acta* **190**, 35–52.

Gomez-Saez, G. V., Dittmar, T., Holtappels, M., Pohlabeln, A. M., Lichtschlag, A., Schnetger, B., et al. (2021). Sulfurization of dissolved organic matter in the anoxic water column of the Black Sea. Science Advances, 7(25), eabf6199.

Hartgers W. A., Lopez J. F., Damste J. S., Reiss C., Maxwell J. and Grimalt J. O. (1997) Sulfur-binding in recent environments: II. Speciation of sulfur and iron and implications for the occurrence of organo-sulfur compounds. *Geochimica et Cosmochimica Acta* **61**, 4769–4788.

689 Hartnett H. E. and Devol A. H. (2003) Role of a strong oxygen-deficient zone in the preservation and
690 degradation of organic matter: A carbon budget for the continental margins of northwest Mexico and
691 Washington State. *Geochimica et Cosmochimica Acta* **67**, 247–264.

692 Hayes J. M. (2001) Fractionation of the isotopes of carbon and hydrogen in biosynthetic processes. In
693 National Meeting of the Geological Society of America. Boston, MA.

694 Heller M. I., Lam P. J., Moffett J. W., Till C. P., Lee J.-M., Toner B. M. and Marcus M. A. (2017)
695 Accumulation of Fe oxyhydroxides in the Peruvian oxygen deficient zone implies non-oxygen
696 dependent Fe oxidation. *Geochimica et Cosmochimica Acta* **211**, 174–193.

697 Hill R. L. (1965) Hydrolysis of Proteins. In *Advances in Protein Chemistry Volume 20* Advances in
698 Protein Chemistry. Elsevier. pp. 37–107.

699 Holmkvist L., Ferdelman T. G. and Jorgensen B. B. (2011) A cryptic sulfur cycle driven by iron in the
700 methane zone of marine sediment (Aarhus Bay, Denmark). *Geochimica et Cosmochimica Acta* **75**,
701 3581–3599.

702 Hülse D., Arndt S. and Ridgwell A. (2019) Mitigation of Extreme Ocean Anoxic Event Conditions by
703 Organic Matter Sulfurization. *Paleoceanography and Paleoclimatology* **34**, 476–489.

704 Ishizuka I. (1997) Chemistry and functional distribution of sulfoglycolipids. *Marine and Petroleum*
705 *Geology* **36**, 245–319.

706 Iversen M. H. and Ploug H. (2013) Temperature effects on carbon-specific respiration rate and sinking
707 velocity of diatom aggregates; potential implications for deep ocean export processes.
708 *Biogeosciences* **10**, 4073–4085.

709 Jessen G. L., Lichtschlag A., Ramette A., Pantoja S., Rossel P. E., Schubert C. J., Struck U. and Boetius
710 A. (2017) Hypoxia causes preservation of labile organic matter and changes seafloor microbial
711 community composition (Black Sea). *Science Advances* **3**, e1601897.

712 Johnston D. T., Gill B. C., Masterson A., Beirne E., Casciotti K. L., Knapp A. N. and Berelson W. (2014)
713 Placing an upper limit on cryptic marine sulphur cycling. *Nature* **513**, 530-533.

714 Jorgensen B. B. (2019) The Biogeochemical Sulfur Cycle of Marine Sediments. *Frontiers in*
715 *Microbiology* **10,** 849.

716 Kamyshny A., Goifman A., Gun J., Rizkov D. and Lev O. (2004) Equilibrium Distribution of Polysulfide
717 Ions in Aqueous Solutions at 25 °C: A New Approach for the Study of Polysulfides' Equilibria.
718 *Environmental Science and Technology* **38**, 6633–6644.

719 Keil R. G., Neibauer J. A., Biladeau C., van der Elst K. and Devol A. (2016) A multiproxy approach to
720 understanding the “enhanced” flux of organic matter through the oxygen-deficient waters of the
721 Arabian Sea. *Biogeosciences* **13**, 2077–2092.

722 Kohnen M., Damste J. S., Haven ten H. L. and De Leeuw J. W. (1989) Early incorporation of
723 polysulfides in sedimentary organic matter. *Nature* **341**, 640–641.

Kohnen M., Sinninghe, Dalen A. K.-V. and De Leeuw J. W. (1991) Di- or polysulphide-bound biomarkers in sulphur-rich geomacromolecules as revealed by selective chemolysis. *Geochimica et Cosmochimica Acta* **55**, 1375–1394.

Kok M. D., Schouten S. and Sinninghe Damsté J. S. (2000) Formation of insoluble, nonhydrolyzable, sulfur-rich macromolecules via incorporation of inorganic sulfur species into algal carbohydrates. *Marine and Petroleum Geology* **64**, 2689–2699.

Kok M., Rijpstra I., Robertson L., Volkman J. K. and Damste J. S. (2000) Early steroid sulfurisation in surface sediments of a permanently stratified lake (Ace Lake, Antarctica). *Geochimica et Cosmochimica Acta* **64**, 1425–1436.

Kutuzov I., Rosenberg Y. O., Bishop A. and Amrani A. (2020) The Origin of Organic Sulphur Compounds and Their Impact on the Paleoenvironmental Record. In *Hydrocarbons, Oils and Lipids: Diversity, Origin, Chemistry and Fate* Springer International Publishing, Cham. pp. 1–54.

La Rocha De C. L. and Passow U. (2007) Factors influencing the sinking of POC and the efficiency of the biological carbon pump. *Deep Sea Research Part II: Topical Studies in Oceanography* **54**, 639–658.

LaLonde R., Ferrara L. and Hayes M. (1987) Low-temperature, polysulfide reactions of conjugated ene carbonyls: A reaction model for the geologic origin of S-heterocycles. *Organic Geochemistry* **11**, 563–571.

Li X., Taylor G. T., Astor Y. and Scranton M. I. (2008) Relationship of sulfur speciation to hydrographic conditions and chemoautotrophic production in the Cariaco Basin. *Marine Chemistry* **112**, 53–64.

Luther G. W., Church T. M., Scudlark J. R. and Cosman M. (1986) Inorganic and Organic Sulfur Cycling in Salt-Marsh Pore Waters. *Science* **232**, 746–749.

Lückge A., Boussafir M., Lallier-Verges E. and Littke R. (1996) Comparative study of organic matter preservation in immature sediments along the continental margins of Peru and Oman. Part I: Results of petrographical and bulk geochemical data. *Organic Geochemistry* **24**, 437–451.

Lyons T. W. (1997) Sulfur isotopic trends and pathways of iron sulfide formation in upper Holocene sediments of the anoxic Black Sea. *Geochimica et Cosmochimica Acta* **61**, 3367–3382.

Lyons T. W., Reinhard C. T. and Planavsky N. J. (2014) The rise of oxygen in Earth's early ocean and atmosphere. **506**, 307–315.

Lyons T. W., Werne J. P., Hollander D. J. and Murray R. W. (2003) Contrasting sulfur geochemistry and Fe/Al and Mo/Al ratios across the last oxic-to-anoxic transition in the Cariaco Basin, Venezuela. *Chemical Geology* **195**, 131–157.

Martin J. H., Knauer G. A., Karl D. M. and Broenkow W. (1987) VERTEX: carbon cycling in the northeast Pacific. *Marine and Petroleum Geology* **34**, 267–285.

Matrai P. A. and Eppley R. W. (1989) Particulate organic sulfur in the waters of the Southern California Bight. *Global Biogeochemical Cycles* **3**, 89–103.

760 Matrai P. A. and Vetter R. D. (1988) Particulate thiols in coastal waters: The effect of light and nutrients
761 on their planktonic production. *Limnology and Oceanography* **33**, 624–631.

762 Metzger K., Rehberger P. A., Erben G. and Lehmann W. D. (1995) Identification and Quantification of
763 Lipid Sulfate Esters by Electrospray Ionization MS/MS Techniques: Cholesterol Sulfate. *Analytical*
764 *Chemistry* **67**, 4178–4183.

765 Mossman J. R., Aplin A. C., Curtis C. D. and Coleman M. L. (1991) Geochemistry of inorganic and
766 organic sulphur in organic-rich sediments from the Peru Margin. *Geochimica et Cosmochimica Acta*
767 **55**, 3581–3595.

768 Overmann J., Beatty J. T., Krause H. R. and Hall K. J. (1996) The sulfur cycle in the chemocline of a
769 meromictic salt lake. *Limnology and Oceanography* **41**, 147–156.

770 Passow U., Alldredge A. L. and Logan B. E. (1994) The role of particulate carbohydrate exudates in the
771 flocculation of diatom blooms. *Marine and Petroleum Geology* **41**, 335–357.

772 Percival E., Rahman M. A. and Weigel H. (1980) Chemistry of the polysaccharides of the diatom
773 Coscinodiscus nobilis. *Marine and Petroleum Geology* **19**, 809–811.

774 Phillips A. A., Wu F. and Sessions A. L. (2021) Sulfur isotope analysis of cysteine and methionine via
775 preparatory liquid chromatography and elemental analyzer isotope ratio mass spectrometry. *Rapid*
776 *Commun. Mass Spectrom.* **35**, 175–24.

777 Pohlabeln A. M., Gomez-Saez G. V., Noriega-Ortega B. E. and Dittmar T. (2017) Experimental Evidence
778 for Abiotic Sulfurization of Marine Dissolved Organic Matter. *Front. Mar. Sci.* **4**, 265.

779 Ramus J. and Groves S. T. (1974) Precursor-Product Relationships during Sulfate Incorporation into
780 Porphyridium Capsular Polysaccharide. *Plant Physiology* **53**, 434–439.

781 Raven M. R., Fike D. A., Bradley A. S., Gomes M. L., Owens J. D. and Webb S. A. (2019) Paired
782 organic matter and pyrite δ34S records reveal mechanisms of carbon, sulfur, and iron cycle
783 disruption during Ocean Anoxic Event 2. *Earth and Planetary Science Letters* **512**, 27–38.

784 Raven M. R., Fike D. A., Gomes M. L. and Webb S. M. (2019) Chemical and Isotopic Evidence for
785 Organic Matter Sulfurization in Redox Gradients Around Mangrove Roots. *Front. Earth Sci.* **7**.

786 Raven M. R., Fike D. A., Gomes M. L., Webb S. M., Bradley A. S. and McClelland H.-L. O. (2018)
787 Organic carbon burial during OAE2 driven by changes in the locus of organic matter sulfurization.
788 *Nature Communications* **9**, 3409.

789 Raven M. R., Keil R. G. and Webb S. M. (2021) Microbial sulfate reduction and organic sulfur formation
790 in sinking marine particles. **371**, 178–181.

791 Raven M. R., Sessions A. L., Adkins J. F. and Thunell R. C. (2016) Rapid organic matter sulfurization in
792 sinking particles from the Cariaco Basin water column. *Geochimica et Cosmochimica Acta* **190**, 175–
793 190.

794 Raven M. R., Sessions A. L., Fischer W. W. and Adkins J. F. (2016) Sedimentary pyrite δ34S differs
795 from porewater sulfide in Santa Barbara Basin: Proposed role of organic sulfur. *Geochimica et*
796 *Cosmochimica Acta* **186**, 120–134.

Resing J. A., Sedwick P. N., German C. R., Jenkins W. J., Moffett J. W., Sohst B. M. and Tagliabue A. (2015) Basin-scale transport of hydrothermal dissolved metals across the South Pacific Ocean. *Nature* **523**, 200–203.

Rickard D. and Luther G. W. (2007) Chemistry of Iron Sulfides. *Chem. Rev.* **107**, 514–562.

Rickard D. and Morse J. (2005) Acid volatile sulfide (AVS). *Marine Chemistry* **97**, 141–197.

Salmon V., Derenne S., Lallier-Verges E., Largeau C. and Beaudoin B. (2000) Protection of organic matter by mineral matrix in a Cenomanian black shale. **31**, 463–474.

Schmidtko S., Stramma L. and Visbeck M. (2017) Decline in global oceanic oxygen content during the past five decades. *Nature* **542**, 335–339.

Shawar, L., Halevy, I., Said-Ahmad, W., Feinstein, S., Boyko, V., Kamyshny, A., & Amrani, A. (2018). Dynamics of pyrite formation and organic matter sulfurization in organic-rich carbonate sediments. Geochimica Et Cosmochimica Acta, 1–73.

Sinninghe Damsté J. S., Irene W., Rijpstra C., De Leeuw J. W. and Schenck P. A. (1988) Origin of organic sulphur compounds and sulphur-containing high molecular weight substances in sediments and immature crude oils. *Organic Geochemistry* **13**, 593–606.

Sinninghe Damsté J. S. and Köster J. (1998) A euxinic southern North Atlantic Ocean during the Cenomanian/Turonian oceanic anoxic event. *Marine and Petroleum Geology* **158**, 165–173.

Stramma L., Prince E. D., Schmidtko S., Luo J., Hoolihan J. P., Visbeck M., Wallace D. W. R., Brandt P. and Körtzinger A. (2011) Expansion of oxygen minimum zones may reduce available habitat for tropical pelagic fishes. *Nature Climate Change* **2**, 33–37.

Suits N. S. and Arthur M. A. (2000) Sulfur diagenesis and partitioning in Holocene Peru shelf and upper slope sediments. *Chemical Geology* **163**, 219–234.

Takano Y., Ito T. and Deutsch C. (2018) Projected Centennial Oxygen Trends and Their Attribution to Distinct Ocean Climate Forcings. *Global Biogeochemical Cycles* **32**, 1329–1349.

Urban N. R., Ernst K. and Bernasconi S. (1999) Addition of sulfur to organic matter during early diagenesis of lake sediments. *Geochimica et Cosmochimica Acta* **63**, 837–853.

van de Velde S. J., Reinhard C. T., Ridgwell A. and Meysman F. J. R. (2020) Bistability in the redox chemistry of sediments and oceans. *Proceedings of the National Academy of Sciences* **483**, 202008235.

van Dongen B. E., Schouten S., Baas M., Geenevasen J. A. J. and Sinninghe Damsté J. S. (2003) An experimental study of the low-temperature sulfurization of carbohydrates. *Organic Geochemistry* **34**, 1129–1144.

Van Mooy B. A. S. and Keil R. G. (2015) Aquatic sample analysis system. U.S. Patent 9,188,512.

Van Mooy B., Keil R. G. and Devol A. H. (2002) Impact of suboxia on sinking particulate organic carbon: Enhanced carbon flux and preferential degradation of amino acids via denitrification. *Geochimica et Cosmochimica Acta* **66**, 457–465.

Vidal-Melgosa S., Sichert A., Ben Francis T., Bartosik D., Niggemann J., Wichels A., Willats W. G. T., Fuchs B. M., Teeling H., Becher D., Schweder T., Amann R. and Hehemann J.-H. (2021) Diatom fucan polysaccharide precipitates carbon during algal blooms. *Nature Communications* **12**, 1150.

Vogt W. (1995) Oxidation of methionyl residues in proteins: tools, targets, and reversal. *Marine and Petroleum Geology* **18**, 93–105.

Webb S. M. (2005) SIXpack: a graphical user interface for XAS analysis using IFEFFIT. *Phys. Scr.* **2005**, 1011.

Webb S. M., McNulty I., Eyberger C. and Lai B. (2011) The MicroAnalysis Toolkit: X-ray Fluorescence Image Processing Software. In the 10th International Conference on X-ray Microscopy. AIP. pp. 196–199.

Webb, S. M.(2020) SIXPACK: a graphical user interface for XAS analysis. Int. Tables Crystallogr. I, https://doi.org/10.1107/S1574870720003456.

Werne J. P., Lyons T. W., Hollander D. J., Chemical M. F. and Sinninghe Damsté J. S. (2003) Reduced sulfur in euxinic sediments of the Cariaco Basin: sulfur isotope constraints on organic sulfur formation. *Marine and Petroleum Geology* **195**, 159–179.

Werne J., Hollander D., Behrens A., Schaeffer P., Albrecht P. and Damste J. (2000) Timing of early diagenetic sulfurization of organic matter: A precursor-product relationship in early Holocene sediments of the anoxic Cariaco Basin, Venezuela. *Geochimica et Cosmochimica Acta* **65**, 1741–1751.

Zerkle A., Kamyshny A., Kump L., Farquhar J., Oduro H. and Arthur M. (2010) Sulfur cycling in a stratified euxinic lake with moderately high sulfate: constraints from quadruple S isotopes. *Geochimica et Cosmochimica Acta* **74**, 4953–4970.

FIGURE CAPTIONS

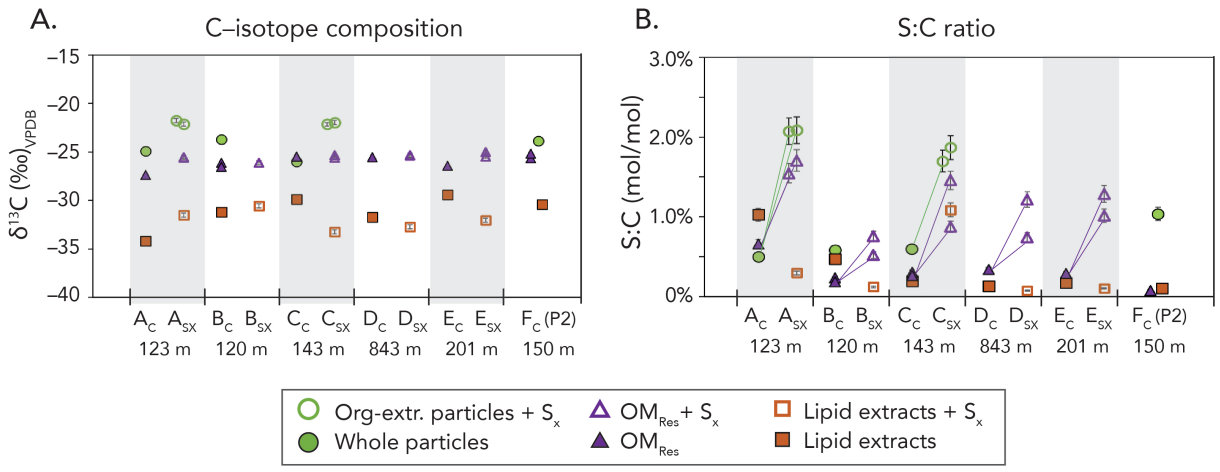

859

860 **Fig. 1: Carbon-isotope composition and molar S:C ratio of particle materials, before and after S_x**
861 **exposure.** S:C ratios exclude inorganic phases (sulfate and FeS) quantified by XAS; uncorrected ratios are
862 reported in Table S2. Filled symbols represent controls (e.g., 'A_C'), and hollow symbols represent
863 experiments (e.g., 'A_{SX}'), as detailed in Table S2. The six discrete sets of samples are listed on the x-axis
864 in arbitrary order. Whole and organic-solvent-extracted particles represent the combination of OM_{Hyd} and
865 OM_{Res}. Samples with multiple symbols represent discrete filter splits rather than replicates of homogenized
866 samples. Error bars indicate the long-term reproducibility of standards (2σ). In panel B, purple and green
867 lines highlight the consistent increase in the S:C ratio of OM_{Res} and whole particle samples following
868 sulfurization; bulk lipids do not show a consistent trend.

869

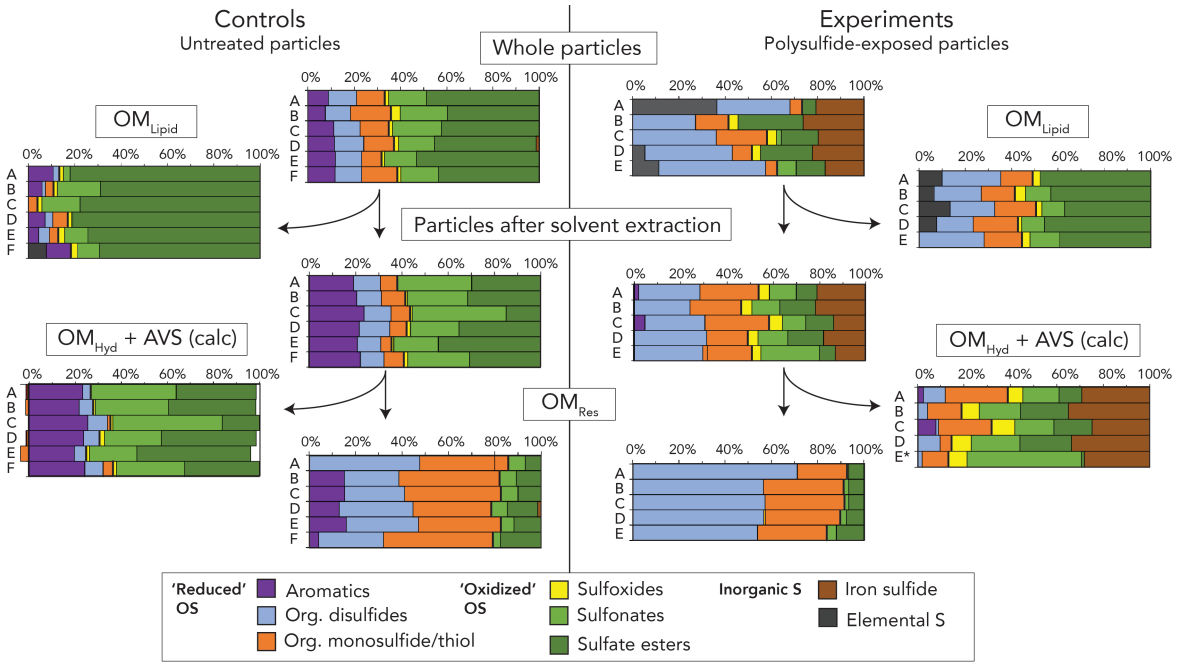

870

871 **Fig. 2 Sulfur speciation in sinking ETNP particles, with and without polysulfide exposure.** Samples
872 A through F represent six separate trap deployments (see Table S1). Heavy black lines between the orange
873 and yellow bars broadly separate 'reduced' from 'oxidized' organic sulfur species. Inorganic sulfate was
874 also detected in samples before hot acidification and is excluded from normalization. Non-sulfate materials
875 lost during hot acidification are calculated by difference using X-ray spectrum step heights and are subject
876 to errors of 5–10%. One sample labeled E* used an assigned step height. Fit uncertainties on each
877 component are typically <2% (see Table S4). The elemental S detected in experimental whole particles
878 (grey) may derive from polysulfide reactants; this was removed from lipid extracts before analysis by Cu
879 exposure.

880

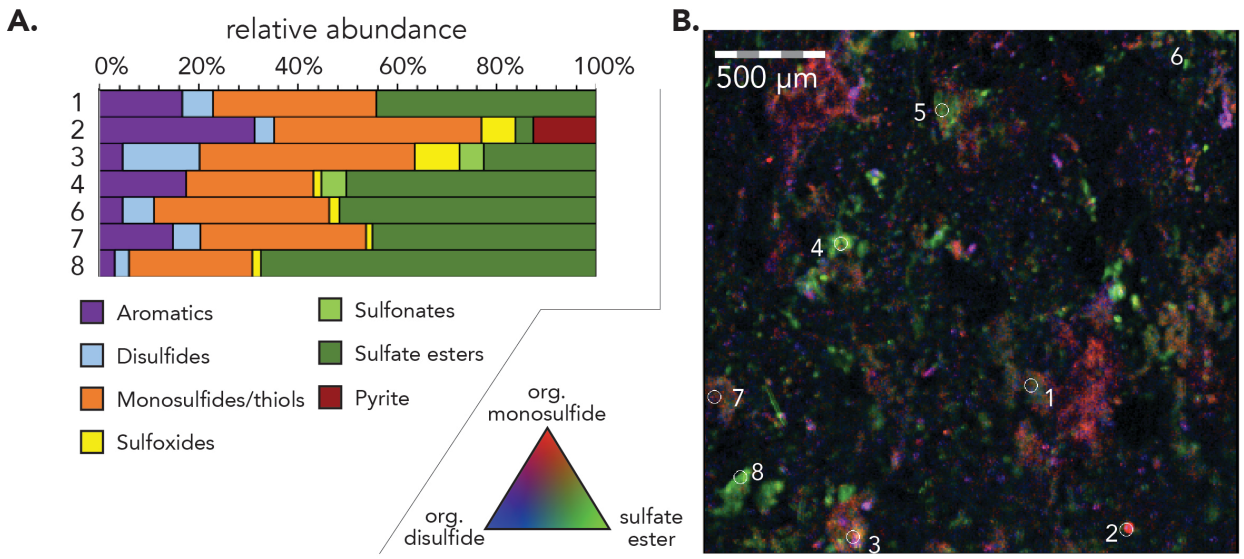

881

882 **Fig. 3 Sulfur speciation of whole particle controls by XAS and XRF.** Particles were collected from
883 site P1 (123 m, sample 'A_C') and are mounted on GFF filters. Panel A: Fitted XAS spectra for specific (~1
884 μm^2) spots, numbered at right. Uncertainties are typically <2%, see Table S5. Panel B: Tri-color XANES
885 fits to multiple-energy maps showing organic monosulfides and thiols (red), disulfides (blue), and sulfate
886 esters (green). Map step size = 7 µm.

887

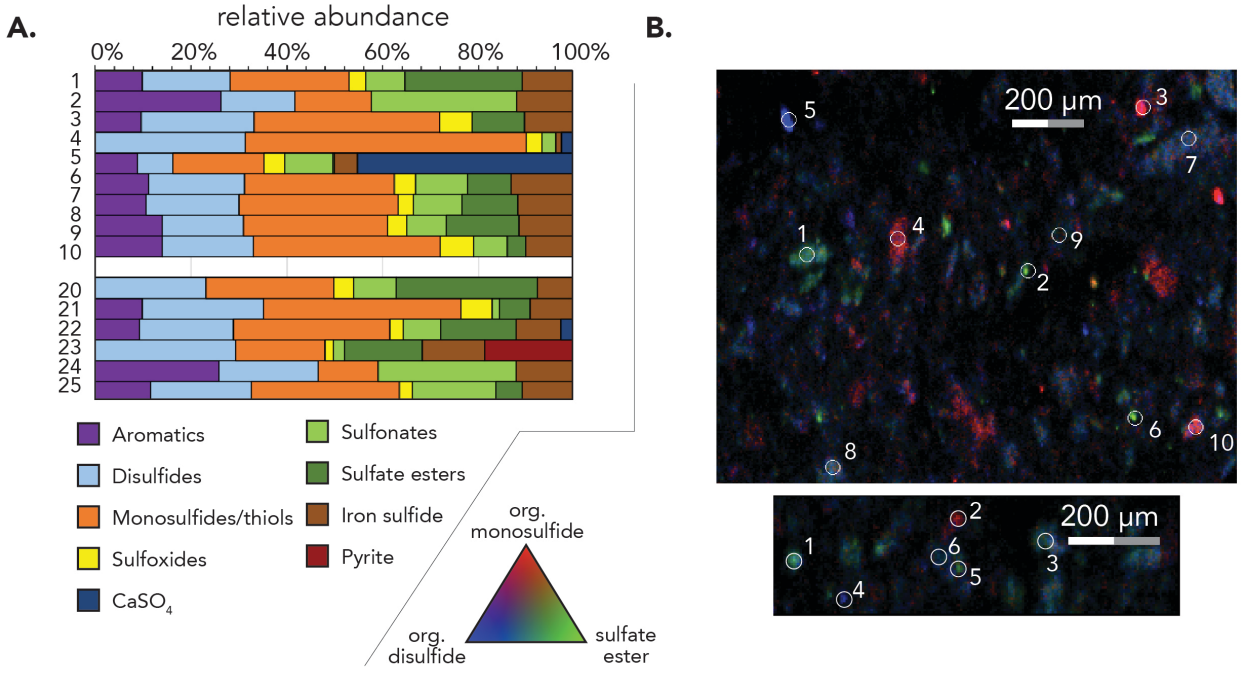

888

Fig. 4 Sulfur speciation maps of polysulfide–exposed particles by XAS and XRF. As in Fig. 3, particles were collected from site P1 (123 m, sample 'A_{Sx}') and are mounted on GFF filters. Panel A: Fitted XAS spectra for specific (~1 μm^2) spots, numbered at right. Uncertainties are typically <2%, see Table S5. Panel B: Tri-color XANES fits to multiple-energy maps from two adjacent filter regions, showing organic monosulfides and thiols (red), disulfides (blue), and sulfate esters (green). Step size = 5 μm. Newly formed disulfides appear as 50-to-100-μm regions surrounding more discrete particles containing various forms of organic S.

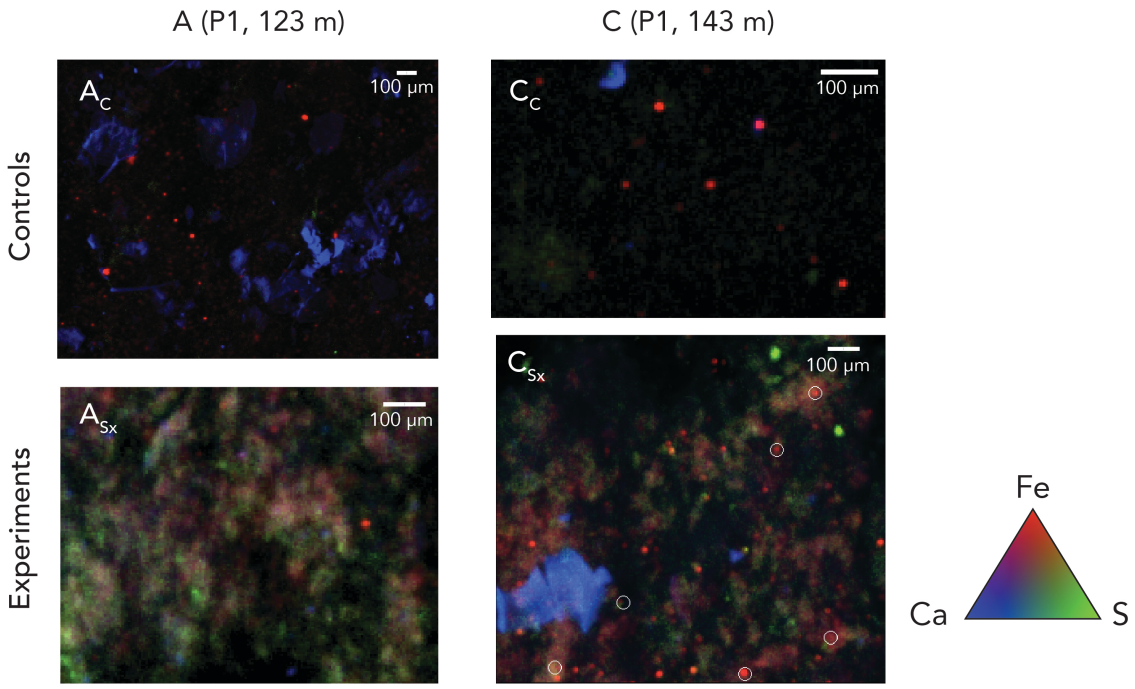

Fig. 5: Maps of iron, calcium, and sulfur on particle filters by XRF. Samples were prepared by washing with buffer under anoxic conditions; sulfur maps in all panels thus include trace inorganic sulfate. Maps show representative regions from sample splits, not the same regions after treatment. Pixels are 5 μm^2. Colors show iron at 7133 eV (red), total calcium (blue), and total sulfur (green).

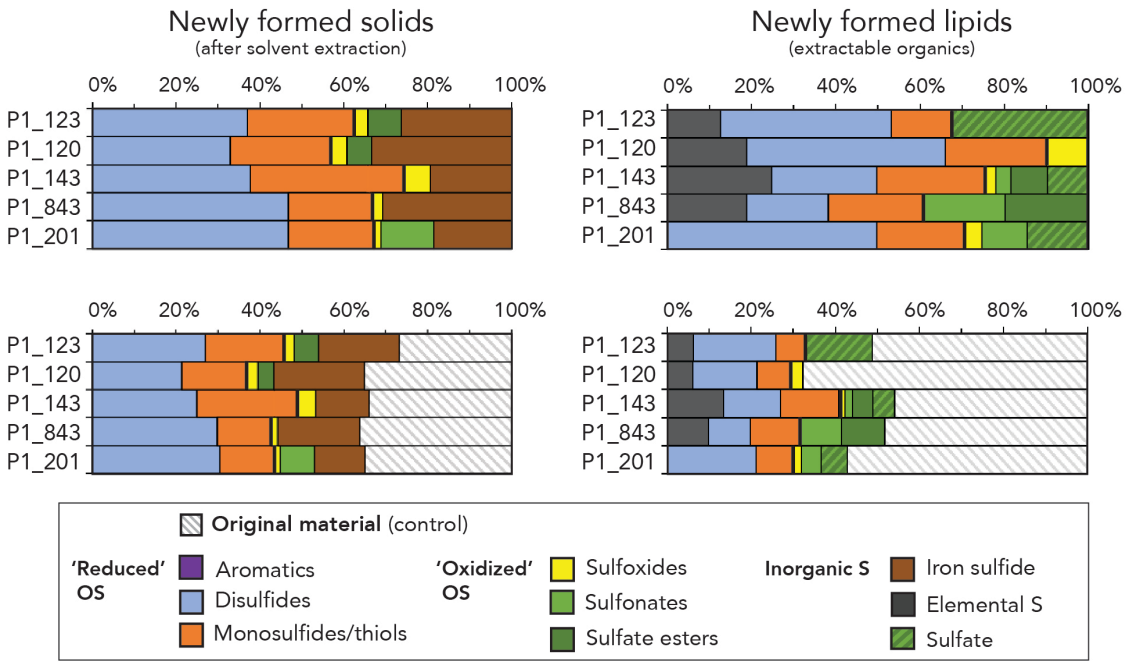

903

904 **Fig. 6 Speciation of products formed during polysulfide exposure.** Heavy black lines broadly separate
905 'reduced' from 'oxidized' organic sulfur species. Results were calculated by linear combination fitting of
906 S_x-exposed sample spectra for solvent-extracted particles (OM_{Res} + OM_{Hyd}, left) and lipid extracts (right)
907 using the control spectra from each sample as a component. Upper and lower panels show the same data,
908 but the lower panel highlights the proportion of S_x-exposed materials that were attributed to pre-existing
909 (control) materials. Newly formed organic S in both pools is largely sulfides and disulfides.

910